Hindawi Publishing Corporation
Advances in Materials Science and Engineering
Volume 2016, Article ID 3905625, 9 pages
http://dx.doi.org/10.1155/2016/3905625

Research Article

Morphology Controlled Synthesis of α-GaO(OH) Nanoparticles: Thermal Conversion to Ga_2O_3 and Photocatalytic Properties

Ayse Dulda

Department of Mechatronics Engineering, Mevlana University, Ardıçlı Mah., Yeni İstanbul Cad. No. 235, Selçuklu, 42250 Konya, Turkey

Correspondence should be addressed to Ayse Dulda; adulda@mevlana.edu.tr

Received 11 November 2015; Accepted 16 February 2016

Academic Editor: Peter Majewski

Morphology controlled α-GaO(OH) particles have been synthesized via precipitation method which allows the tuning of relative growth rates of crystal facets. The effects of alkali addition rate and the type of alkali on the growth rates of the crystal facets during hydrolysis were also investigated. XRD and TG analysis confirmed that there was a phase transition from GaO(OH) to Ga_2O_3 when precursor sample was calcined to 750°C. The single phase α-Ga_2O_3 was obtained after thermal treatment of NaOH precipitated precursor, while β-Ga_2O_3 was formed when the urea or NH_4OH precipitated precursor was calcinated. Furthermore, the thermal, spectral, and photocatalytic properties connected to the crystal structure and morphology were discussed.

1. Introduction

Recently, wide band gap transparent conductive oxides (TCO) attracted great attention due to their applicability in diverse fields from catalysis to biotechnology. Semiconducting oxides, especially of band gap larger than 4 eV, are promising for the newly developed UV optoelectronic devices such as Thin Film Transistor (TFT), Solar Cells, UV LEDs, displays, and sensors [1–3]. For example, ITO conventional TCO electrode is opaque in the deep UV region (~300 nm) due to its small band gap energy (~3.2 eV) while wide band gap semiconducting oxide such as Ga_2O_3 with a band gap of 4.8–4.9 eV is transparent to deep UV light. Hence, Ga_2O_3 as a new TCO electrode can play a major role in increasing the performance of many optoelectronic devices. Researchers have employed Ga_2O_3 as a new TCO [4] in various other applications [5–7]. Orita et al. reported Ga_2O_3 to be the best candidate for a new TCO, because it shows high transmittance to deep UV, presents controlled electrical conductivity, and is thermally stable even when applied to high voltage [4]. Oshima et al. used Ga_2O_3 as a TCO to fabricate deep UV photo detector [5]. Matsuzaki et al. fabricated Field Effect Transistor (FET) using the Ga_2O_3 films for the channel in Metal-Insulator-Semiconductor (MIS) structure [3]. Applications of Ga_2O_3 are not limited to optoelectronic device. The large band gap of Ga_2O_3 is believed to be an important factor that contributes to a superior photocatalytic performance. Hou et al. reported that Ga_2O_3 when used as a catalyst over benzene presents a better photocatalytic property than that of commercial TiO_2 [6]. Due to the structure stability and electronic conductivity at high temperature, β-Ga_2O_3 was pointed out to be good candidate for gas sensor applications. Ogita et al. reported that Ga_2O_3 based gas sensor works with superior performance at high temperatures of more than 600°C [7]. Ga_2O_3 has also been widely used as a host material for phosphors [8]. And because Ga_2O_3 has a strong redox ability to produce radical oxygen species, considering DNA and proteins absorption/fluorescence ability in deep UV region, we believe that Ga_2O_3 nanostructured materials can be a powerful theragnostic agent for future light based therapy and diagnosis.

Size and shape of nanoparticles such as Ga_2O_3 are very important factor for those aforementioned applications. For example, spherical shape nanoparticles less than 20 nm are preferred in biological applications. However for phosphor application, micron size particles give better luminescence intensity [9]. On the other hand, shape is very important

for photocatalysis since large surface area contributes to high redox ability [10]. Therefore, size and shape controlled synthesis of these nanoparticles is highly needed. The most common approach for controlling the size and shape of nanoparticles (monodisperse nanoparticles) is the hydrolysis of metal salts from homogenous solution in either the presence or absence of a surfactant. Cüneyt Taş et al. synthesized quadrilateral prisms and spindle-like gallium oxide hydroxide ($GaOOHxH_2O$) single crystals by hydrolysis of Ga^{3+} ions in the presence of decomposing urea [11]. Matijević and Hsu observe effect of surfactant on agglomeration by preparing Gd_2O_3 nanoparticles via surfactant free and surfactant assisted homogenous precipitation method [12]. Hemmer et al. prepared Gd_2O_3 nanoparticles through hydrolysis reactions with morphology controlling surfactant (CTAB and PEG) [13]. Chen and Chang reported that the addition of low dielectric medium to the aqueous solution could change the thermodynamics of reaction system and nucleation kinetics [14]. Yoo et al. prepared spherical monodisperse nanoparticles in a low dielectric medium [15]. Moscolo et al. studied the effect of slow or fast alkaline addition on the precipitation kinetics of iron chloride solution in a large pH window using different bases [16].

In this study, our objective is to investigate the effect of addition rate of alkali and the type of used alkali on the particle growth and the implications of final size and morphology on the photocatalytic property of Ga_2O_3.

2. Synthesis

2.1. Chemicals. $GaCl_3$ (ultra dry 99.99% Abcr), urea (>99% pure, Merck), sodium hydroxide (reagent grade, ≥98%, pellets anhydrous Sigma-Aldrich), and ammonia solution (25% Merck) were used without further purification.

2.2. Procedure. For the alkaline precipitation, 25 g $GaCl_3$ (ultra dry 99.999% Abcr) was dissolved in 100 mL deionized water. An aqueous NaOH solution (c = 0.5 mol/L, V = 100 mL) or (1000 μL) ammonia solution was added to the $GaCl_3$ solution and vigorously stirred and centrifuged at room temperature.

For the homogeneous precipitation, 758.3 mg (1.68 mmol) $GaCl_3$ was dissolved in 250 mL H_2O and 9.01 g (150 mmol) urea was added to the pure solution and the mixture was kept stirring for 10 min. For precipitation, the mixture was stirred at 85°C for 30–45 min. When solution pH reached 5, the solution was cooled to room temperature in an ice bath and centrifuged with 15000 rpm to collect resulting nanoparticles. The above obtained fresh precipitates were dried at room temperature and fired at 750°C for 1 h.

2.3. Instrumentation. The crystalline phase of the samples was determined by powder X-Ray diffraction method using a Bruker D8 Advance X-ray diffractometer with CuKα radiation. A scan rate of 2° 2θ/min was set over the range of 10–75°. The morphological characterization of the samples was monitored using scanning electron microscopy (Zeiss LS-10 GmbH, Germany).

Thermogravimetric and differential thermal analysis of samples was performed (Mettler Toledo TGA/DSC 2 Star System) in an air atmosphere at a heating rate of 5°C/min up to 1000°C.

Fourier transform infrared (FT-IR) spectra were recorded on a Tensor 27 spectrometer (Bruker Optics, Wissembourg, France). It was equipped with a horizontal attenuated total reflectance (ATR) accessory composed of a ZnSe.

UV-vis absorption spectra were recorded using a Shimadzu UV-1800 spectrophotometer in the wavelength range of 250–800 nm.

2.4. Photodegradation Measurement. First, 240 mL of RB solution with a concentration of 6 mg/L was prepared. Total 6 samples (GaO(OH) and Ga_2O_3) were weighed for photodegradation measurements. 20 mg of each sample was separately added to 40 mL of the above RB containing solutions and kept for 30 min in the dark with mechanical stirring. An 8 W lamp (Phillips, UVC 254 nm made in Poland) was placed at 20 cm above the mixed solutions. To measure photocatalytic degradation of RB, each solution was taken out at 15 min intervals by pipet and centrifuged to separate nanoparticles from RB containing solution. UV-vis adsorption spectra were recorded at different intervals to monitor the degradation process (absorption max. of RB at 554 nm) using a Shimadzu UV-1800 spectrophotometer.

3. Results and Discussions

3.1. Morphology and Crystallinity. Size and morphology control of α-GaOOH nanoparticles were reported by previous researchers via hydrolysis by varying the pH, temperature, anion concentration, and aging time of metal salt solutions in the presence or absence of a surfactant. In most of these studies, hydrolysis of the metal salt solutions was typically achieved by dropwise addition of an alkali such as NaOH, KOH, NH_4OH, and Na_2CO_3 [17]. Dropwise addition involves addition of a single drop of an alkali one at a time repeatedly until the needed pH level is reached. In this research, instead of the dropwise addition method, a new strategy is devised that involves one time addition of the alkali needed to reach a specific pH. Experiments were conducted to verify the effect of the addition rate and effect of the alkali type on particle size and morphology. At first, experiments were conducted to verify the effect of pH on morphology and aspect ratio. Figure 1 shows the morphology of GaO(OH) precipitates obtained via hydrolysis from $GaCl_3$ solution with dropwise addition of dilute ammonia (NH_4OH, 25% Merck) solution at (a) pH = 4, (b) pH = 6, (c) pH = 8, and (d) pH = 10. Our results agreed with previous reports indicating effect of pH on morphology and aspect ratio [11, 18]. It can be observed in all these results that spheroidal shape nanoparticles were obtained and their morphology did not change from acidic to basic region. However, except for pH = 8, the aspect ratio of nanoparticles increased. At a pH value of 4.0, spheroidal shape nanoparticles 1.35 μm in length and 550 nm in width were observed (Figure 1(a)). When the pH value increased to 6 the aspect ratio of nanoparticles increased from 2.43 to 3.35 and nanoparticles length and width were 1.3 μm and 400 nm,

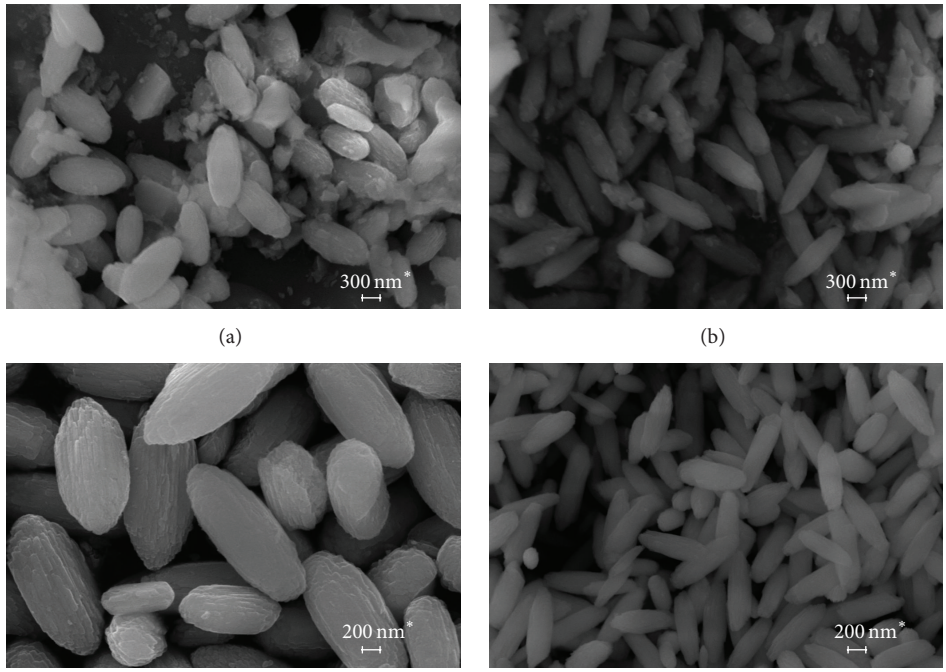

Figure 1: SEM images of GaO(OH) crystals prepared by alkali (NH_4OH) precipitation of $GaCl_3$ solution at (a) pH = 4, (b) pH = 6, (c) pH = 8, and (d) pH = 10.

respectively (Figure 1(b)). At a pH value of 8 and average length and width of 2.05 μm and 900 nm, nanoparticles were observed with average aspect ratio of 2.27 (Figure 1(c)). When the pH value further increased to 10, resulting nanoparticles were 1.24 μm in length and 390 nm in width with average aspect ratio of 3.19 (Figure 1(d)). Our results indicated that, regardless of pH, when alkali solution was injected slowly into the system, spheroidal nanoparticles were formed. The structure of α-GaOOH consists of double chains of edge-shared octahedra where Ga^{3+} ions are surrounded by six oxygen ions and its preferential growth direction lies along the c-axis by the continuous linking of the $Ga^{3+}O_6$ octahedra [11, 18]. In principle, a crystal plane with more closely packed atoms has lower density of the unsaturated bonds and thus a lower specific surface free energy. Based on the gallium atom density difference, crystal plane surface energies from highest to lowest are {001} (along length), {010} (along width), and {100} (along thickness), respectively. Due to the slow hydrolysis of gallium chloride solution through the dropwise addition of ammonia, the facet (001) of GaO(OH) crystal has a preference to absorb OH^{-1} ions. As the OH^{-1} ion concentration increases from acidic to basic region, growth rate along ⟨001⟩ (longitudinal direction of the α-GaO(OH) nanocrystal) is faster than ⟨010⟩ and ⟨100⟩ [18–20]. The growth rates along various crystallographic directions can be controlled by the selective adsorption ability of each crystal facet [20, 21]. Scheme 1 presents an overview of synthesis routes and how variations in synthesis conditions affect morphology and size of the resultant nanoparticles. Here we performed the experiments to understand the effect of alkali addition rate and type of alkali on the growth rates of crystal facets. Figure 2 shows GaO(OH) nanoparticles obtained through the hydrolysis with (a) urea at pH 5, (b) fast addition of ammonia at pH 8, and (c) fast addition of NaOH at pH 8. Decomposition rate of urea is slower than dropwise addition ammonia. Therefore, more uniform spheroidal shaped GaO(OH) nanoparticles with an average length 600 nm and width 200 nm were formed from decomposition of urea at pH 5 (Figure 2(a)). In Figure 2(b), spherical shape nanoparticles were observed and particle size decreased to 300 nm in diameter with fast addition of ammonia. It was realized that addition of all alkali at once with vigorous stirring resulted in equal adsorption of OH^{-1} ions from each crystal facet. After nucleation, each crystal facet had almost the same probability to grow and thus spherical shaped nanoparticles were formed [20]. In addition, it is expected that when the alkali addition rate is fast, the solution reaches supersaturation state rapidly. This leads to the formation of large number of initial nuclei at the nucleation stage, resulting in large number of particles with smaller size [22]. Besides the intrinsic anisotropy in GaO(OH) crystal, the growth rates of each crystal facet can be manipulated by means of adsorption of capping ions or molecules on specific crystal facets [23, 24]. Figure 2(c) shows the effect of the type of alkali on the particle size and morphology. It can be observed that spherical shape nanoparticles were formed and a further decrease in particle size (~150 nm) was obtained when ammonia solution was replaced by NaOH. This is because the sodium ion is smaller than the ammonium cation. Due to its small hydration sphere in solution, sodium ion can easily be adsorbed onto all

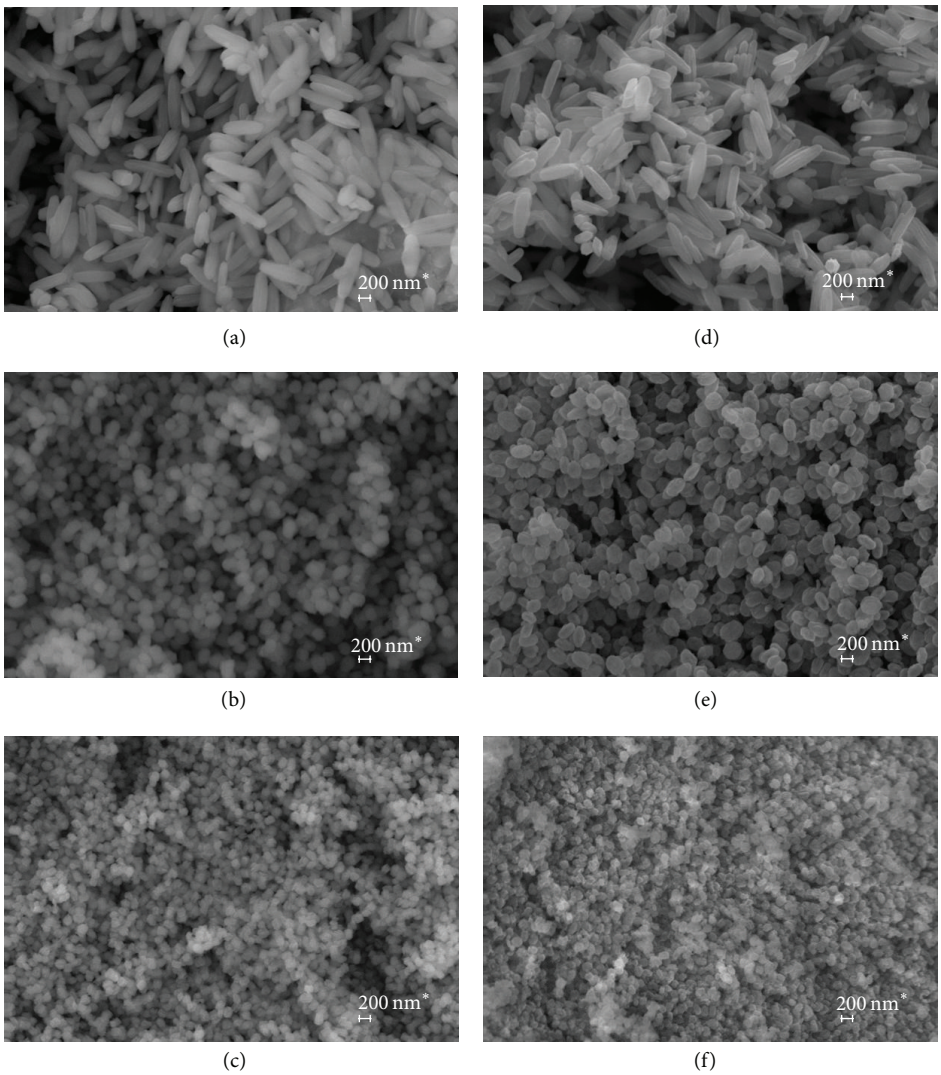

Figure 2: SEM images of GaO(OH) crystals precipitated from $GaCl_3$ solution with (a) decomposition of urea, (b) NH_4OH, and (c) NaOH; SEM images of Ga_2O_3 crystals after thermal conversion of (d) urea precipitated, (e) NH_4OH precipitated, and (f) NaOH precipitated GaO(OH) crystals.

the crystal facets without any selectivity and thus hindering subsequent growth [25].

After calcination at 750°C almost all samples preserved their particle size and morphology (Figures 2(d), 2(e), and 2(f)). The crystalline structure and phase purity of the synthesized samples were examined by powder XRD pattern. Figure 3 shows the XRD patterns of precursor (GaO(OH)) and calcined (Ga_2O_3) samples obtained through the hydrolysis with urea, ammonia, and NaOH, respectively. Precursor samples prepared by urea, NH_4OH, and NaOH displayed sharp and narrow peaks indicating the high crystallinity of obtained nanoparticles (Figures 3(a), 3(b), and 3(c)). Peak positions of precursor samples well matched with orthorhombic phase of α-GaO(OH) (JCPDS card number 01-071-2778) [26]. Both XRD and TGA results confirmed that there was a phase transition from GaO(OH) to Ga_2O_3 when precursor sample was calcined to 750°C. The sample prepared with hydrolysis of NaOH displayed rhombohedral polymorph of Ga_2O_3 (JCPDS card number 06-0503) after calcination (Figure 3(d)). Other calcined samples prepared by NH_4OH and urea (Figures 3(e) and 3(f)) agreed with monoclinic phase of β-Ga_2O_3 (JCPDS card number 11-0370) [11]. Lower crystallinity of NaOH precipitated sample can be attributed to a higher phase transformation temperature connected to particle size.

3.2. TG/DTA Analysis. Figure 4 shows the TGA/DTA curves of GaO(OH) precipitates obtained by hydrolysis of gallium chloride aqueous solutions with (a) urea, (b) NH_4OH, and (c) NaOH. DTA results of urea precipitated sample demonstrate that there were two endothermic peaks during the temperature increment up to 800°C with 18.4 wt% total weight loss. These endothermic peaks at around 182°C and 378°C can

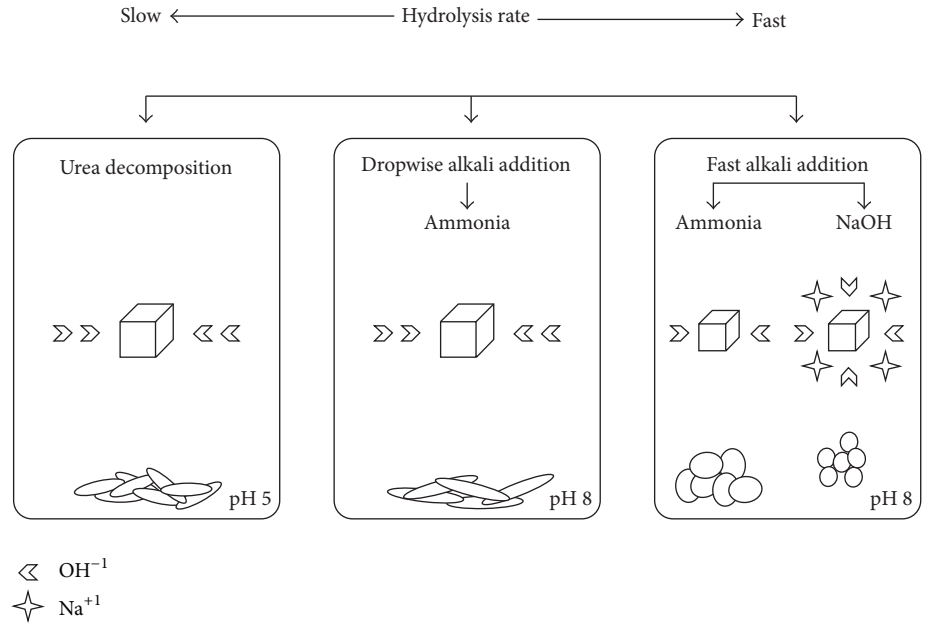

Scheme 1: An overview of the synthesis routes and crystal growth mechanism.

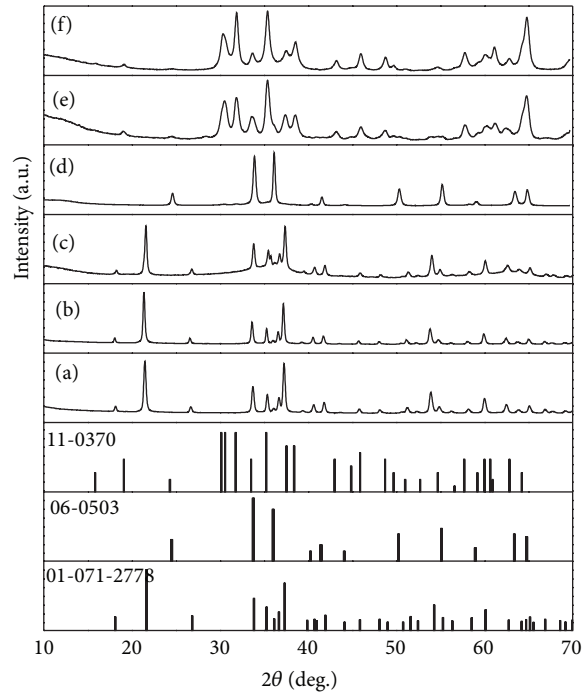

Figure 3: XRD diffraction pattern of GaO(OH) crystals precipitated from $GaCl_3$ solution with (a) NaOH, (b) NH_4OH, and (c) decomposition of urea; XRD diffraction pattern of Ga_2O_3 crystals after thermal conversion of GaO(OH) crystals hydrolysed with (d) NaOH, (e) NH_4OH, and (f) urea.

be assigned to simultaneous dehydration and decomposition of residual carbonates. Beyond 480°C there was no significant difference in weight loss with increase in temperature. However there was a strong exothermic peak between 700°C and 750°C indicating phase transformation to β-Ga_2O_3. Urea precipitated sample displayed higher weight loss compared to the precipitation with NH_4OH (11.89 wt%) and NaOH (10.94 wt%). A higher weight loss in urea precipitated sample was probably caused by higher water content and amorphous gallium hydroxide phase which is also confirmed by XRD with slightly lower crystallinity (Figure 3(a)) [27]. In addition, urea precipitated sample contains residual carbonates [11].

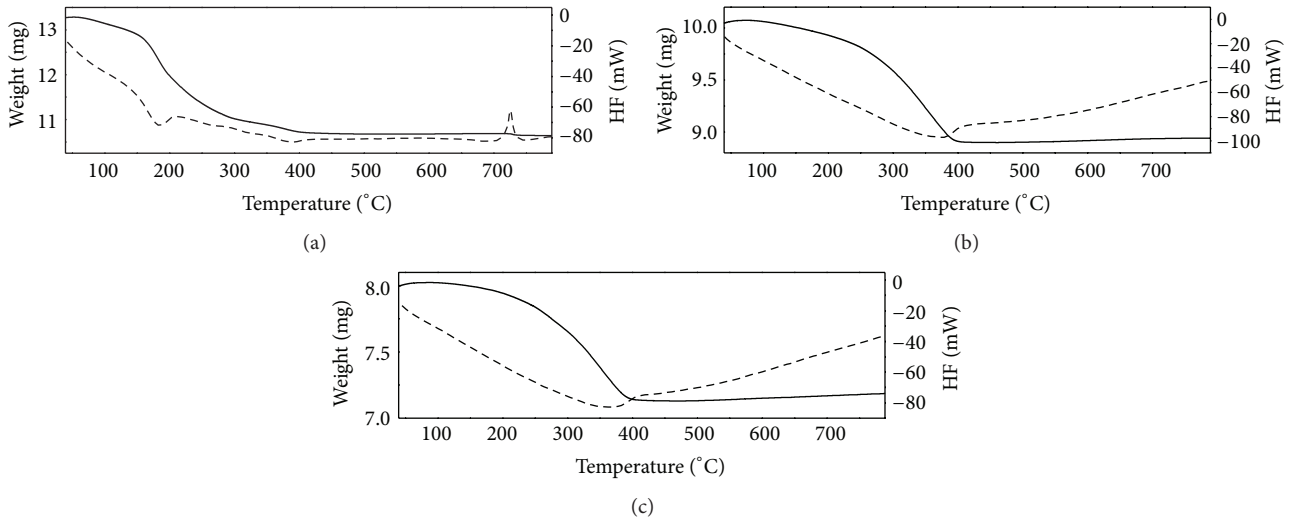

Figure 4: TGA/DTA curves of α-GaO(OH) nanoparticles obtained in aqueous solution through hydrolysis with (a) urea, (b) NH_4OH, and (c) NaOH.

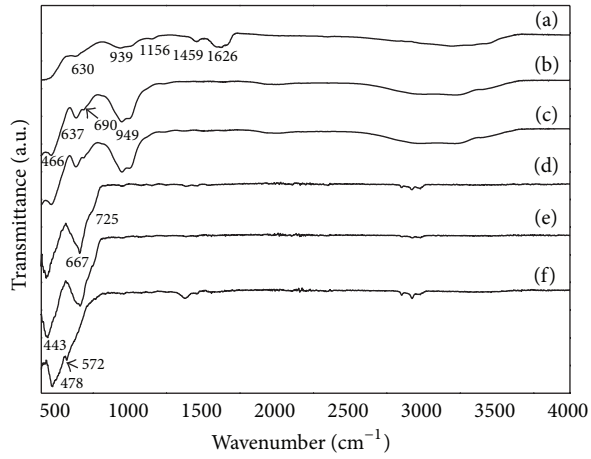

Figure 5: FT-IR spectra of GaO(OH) crystals precipitated from $GaCl_3$ solution with (a) decomposition of urea, (b) NH_4OH, and (c) NaOH; FT-IR spectra of Ga_2O_3 crystals after thermal conversion of GaO(OH) crystals hydrolysed with (d) urea, (e) NH_4OH, and (f) NaOH.

NH_4OH precipitated sample displayed a higher weight loss compared to NaOH precipitated one. This can be attributed to larger cation size of ammonia which cannot easily be adsorbed from crystal facets [25]. Therefore adsorption of OH^- ions or intercalation of water into crystal structure is more favoured.

3.3. FT-IR Analysis. The FT-IR spectra of α-GaO(OH) nanoparticles prepared by hydrolysis with urea, NH_4OH, and NaOH and their calcined powders at 750°C are given in Figure 5. It was reported that particle size and shape are an important factor that determines the position of IR-bands due to the polarization charge induced at the particle surface by an external electromagnetic field when the particle dimensions are smaller than the wavelength of the incident radiation. Krehula et al. and Wang et al. reported the effect of the particle size, shape (aspect ratio), and internal structure on the infrared absorption spectra of α-Ga_2O_3 and β-Ga_2O_3 particles [27, 28].

They observed that as the particle size and aspect ratio decreased infrared absorptions of nanoparticles shifted to lower frequencies. Figure 5(a) shows a broad H-O-H stretching at around 3400 cm^{-1} and bending mode of H-O-H at around 1626 cm^{-1} due to the adsorbed water molecules. The presence of carbonate group in this sample was confirmed by characteristics bands of ν_{as} O-C-O (1459 cm^{-1}). The bands at around 939 and 630 cm^{-1} were assigned to constitutional Ga-OH bending mode and these bands shifted to 949 and 637 cm^{-1} in the spectrum of NH_4OH (Figure 5(b)) and NaOH (Figure 5(c)) precipitated samples [11, 26]. The IR absorption at 466 cm^{-1} could be assigned to vibrations of the Ga-O bonds in GaO_6 octahedra. The monoclinic phase of β-Ga_2O_3 has C2/m symmetry and Ga atoms have tetrahedral- and octahedral-like coordination in the lattice. Therefore

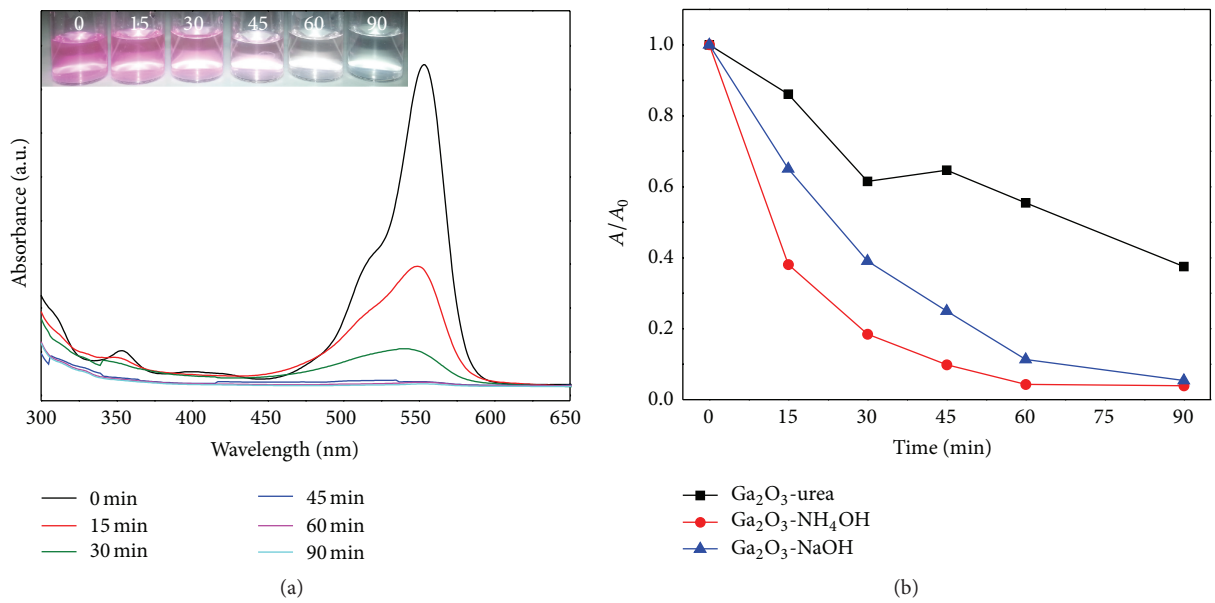

FIGURE 6: (a) The UV-visible absorption spectra of RhB solution in the presence of Ga_2O_3 crystals (prepared by the precipitation of $GaCl_3$ solution with NH_4OH) under UVC light (254 nm) irradiation; (b) photodegradation curve of Ga_2O_3 samples as a function of irradiation time.

two stretching modes of Ga-O bonds associated with GaO_6 octahedra and GaO_4 tetrahedra at 667 cm^{-1} and 730 cm^{-1} were observed in Figures 5(d) and 5(e), respectively. The rhombohedral phase of α-Ga_2O_3 has the corundum structure with R $\bar{3}$ c symmetry. The oxygen ions are approximately hexagonally close packed and the gallium ions occupy two-thirds of the octahedral sites. Each Ga octahedron shares one face and three edges with three other octahedra; the Ga octahedra are moderately distorted in the lattice. Two peaks at 478 and 572 cm^{-1} can be assigned to vibrations of the Ga-O bonds in GaO_6 octahedra (Figure 5(f)) [29].

3.4. Photocatalytic Activity. The photocatalytic activity of the catalyst depends on the crystallinity, surface area, band gap energy, absorption ability towards the reactants, and the separation or the transportation rate of photogenerated electron/hole pairs [30]. The photocatalytic activities of α-GaO(OH), α-Ga_2O_3, and β-Ga_2O_3 nanoparticles were evaluated by the photocatalytic degradation of Rhodamine Blue (RB) under UVC (254 nm) irradiation. Figure 6(a) shows absorption spectra of RB solution in the presence of β-Ga_2O_3 nanoparticles. The major absorption band of RB at 554 nm decreased as a function of irradiation time and almost disappeared after 90 min. Inset shows the time dependent photographs of solution after UVC irradiation. This sample was obtained by thermal conversion of ammonia precipitated GaO(OH) nanoparticles at 750°C as shown in Figure 2(e). In comparison to the spheroidal shaped β-Ga_2O_3 nanoparticles (600 nm in length), the spherical shaped β-Ga_2O_3 nanoparticles (300 nm in diameter) displayed higher activity (Figure 6(b)). As the surface area increases by decreasing particle size, higher photocatalytic activity can be obtained due to the larger contact area between photocatalyst and target material. Although the particle size of NaOH precipitated sample is much smaller than NH_4OH precipitated sample (Figures 3(d) and 3(e)) higher activity of NH_4OH precipitated sample can be attributed to its higher crystallinity (Figure 4) [31, 32]. Absorption spectra of a solution of RB in the presence of α-GaO(OH) nanoparticles prepared by hydrolysis with urea are given in Figure 7(a). Under the irradiation of UVC light for 90 min, only 3% of RB is degraded. All α-GaO(OH) nanoparticles prepared by hydrolysis with urea, NH_4OH, and NaOH displayed similar behaviour. Low photocatalytic activity of α-GaOOH was probably originated by its large band gap energy. According to previous report estimated optical band gap value for α-GaOOH (E_g = 5.27 eV) was higher than those of α-Ga_2O_3 (4.98 eV) or β-Ga_2O_3 (4.8 eV) [33]. Therefore for the degradation of RB in the presence of α-GaOOH nanoparticles light energy should be higher than UVC (254 nm) irradiation.

4. Conclusions

α-GaO(OH) particles of various sizes and shapes were synthesized via precipitation method by controlling the growth kinetics of crystal facets. Our results indicated that type of alkali and rate of alkali addition into gallium(III) chloride solution had a great influence on nucleation and growth kinetics and thus on morphology. Spheroidal morphology was observed when gallium(III) chloride hydrolysed with dropwise addition of ammonia at wide pH range (4, 6, 8, and 10). Similar spheroidal morphology was obtained by uniform and slow release of OH^{-1} ions from decomposing urea. Preferential growth directions were suppressed by controlling

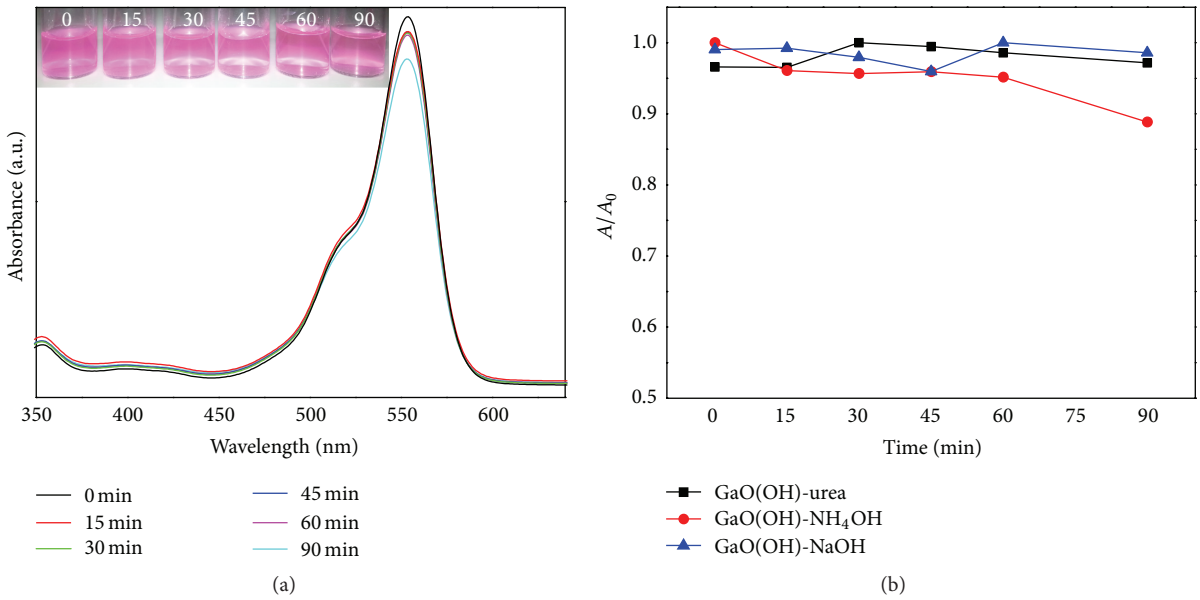

FIGURE 7: (a) The UV-visible absorption spectra of RhB solution in the presence of GaO(OH) crystals (prepared by the precipitation of $GaCl_3$ solution with urea) under UVC light (254 nm) irradiation; (b) photodegradation curve of GaO(OH) samples as a function of irradiation time.

the rate of alkali addition and spherical morphology was observed with fast addition of NH_4OH or NaOH. Crystallite size decreased when NaOH was replaced by NH_4OH. This indicated that type of alkali and precipitation kinetics had great influence on morphology. XRD and TGA analysis confirmed that there was a phase transition from GaO(OH) to Ga_2O_3 when precursor sample was calcined to 750°C. The single phase α-Ga_2O_3 was obtained after thermal treatment of NaOH precipitated precursor, while β-Ga_2O_3 was formed from urea or NH_4OH precipitated precursor. Lower crystallinity of NaOH precipitated sample can be attributed to a higher phase transformation temperature connected to particle size. The morphology of fresh GaO(OH) precipitates was maintained even after thermal treatment at 750°C. In comparison to the spheroidal shaped β-Ga_2O_3 nanoparticles (600 nm in length), the spherical shaped β-Ga_2O_3 nanoparticles (300 nm in diameter) displayed higher activity. All α-GaO(OH) nanoparticles prepared by hydrolysis with urea, NH_4OH, and NaOH displayed similar behaviour. Low photocatalytic activity of α-GaOOH was probably originated by its large band gap energy.

Conflict of Interests

The author declares that there is no conflict of interests regarding the publication of this paper.

Acknowledgment

This work was supported by the TUBITAK under Project no. 113M899.

References

[1] N. Ueda, H. Hosono, R. Waseda, and H. Kawazoe, "Synthesis and control of conductivity of ultraviolet transmitting β-Ga_2O_3 single crystals," *Applied Physics Letters*, vol. 70, no. 26, pp. 3561–3563, 1997.

[2] K. Matsuzaki, H. Yanagi, T. Kamiya et al., "Field-induced current modulation in epitaxial film of deep-ultraviolet transparent oxide semiconductor Ga_2O_3," *Applied Physics Letters*, vol. 88, no. 9, Article ID 092106, 2006.

[3] K. Matsuzaki, H. Hiramatsu, K. Nomura et al., "Growth, structure and carrier transport properties of Ga_2O_3 epitaxial film examined for transparent field-effect transistor," *Thin Solid Films*, vol. 496, no. 1, pp. 37–41, 2006.

[4] M. Orita, H. Ohta, M. Hirano, and H. Hosono, "Deep-ultraviolet transparent conductive β-Ga_2O_3 thin films," *Applied Physics Letters*, vol. 77, no. 25, pp. 4166–4168, 2000.

[5] T. Oshima, T. Okuno, and S. Fujita, "Ga_2O_3 thin film growth on c-plane sapphire substrates by molecular beam epitaxy for deep-ultraviolet photodetectors," *Japanese Journal of Applied Physics*, vol. 46, no. 11, pp. 7217–7220, 2007.

[6] Y. Hou, X. Wang, L. Wu, Z. Ding, and X. Fu, "Efficient decomposition of benzene over a β-Ga_2O_3 photocatalyst under ambient conditions," *Environmental Science & Technology*, vol. 40, no. 18, pp. 5799–5803, 2006.

[7] M. Ogita, K. Higo, Y. Nakanishi, and Y. Hatanaka, "Ga_2O_3 thin film for oxygen sensor at high temperature," *Applied Surface Science*, vol. 175-176, pp. 721–725, 2001.

[8] T. Miyata, T. Nakatani, and T. Minami, "Gallium oxide as host material for multicolor emitting phosphors," *Journal of Luminescence*, vol. 87–89, pp. 1183–1185, 2000.

[9] K. Kömpe, H. Borchert, J. Storz et al., "Green-emitting $CePO_4$:Tb/$LaPO_4$ core-shell nanoparticles with 70% photoluminescence quantum yield," *Angewandte Chemie—International Edition*, vol. 42, no. 44, pp. 5513–5516, 2003.

[10] J. Sun, L. Gao, and Q. Zhang, "Synthesizing and comparing the photocatalytic properties of high surface area rutile and anatase titania nanoparticles," *Journal of the American Ceramic Society*, vol. 86, no. 10, pp. 1677–1682, 2003.

[11] A. Cüneyt Taş, P. J. Majewski, and F. Aldinger, "Synthesis of gallium oxide hydroxide crystals in aqueous solutions with or without urea and their calcination behavior," *Journal of the American Ceramic Society*, vol. 85, no. 6, pp. 1421–1429, 2002.

[12] E. Matijević and W. P. Hsu, "Preparation and properties of monodispersed colloidal particles of lanthanide compounds. I. Gadolinium, europium, terbium, samarium, and cerium(III)," *Journal of Colloid And Interface Science*, vol. 118, no. 2, pp. 506–523, 1987.

[13] E. Hemmer, N. Venkatachalam, H. Hyodo, and K. Soga, "The role of pH in PEG-*b*-PAAc modification of gadolinium oxide nanostructures for biomedical applications," *Advances in Materials Science and Engineering*, vol. 2012, Article ID 748098, 15 pages, 2012.

[14] H.-I. Chen and H.-Y. Chang, "Homogeneous precipitation of cerium dioxide nanoparticles in alcohol/water mixed solvents," *Colloids and Surfaces A: Physicochemical and Engineering Aspects*, vol. 242, no. 1–3, pp. 61–69, 2004.

[15] H. S. Yoo, H. S. Jang, W. B. Im, J. H. Kang, and D. Y. Jeon, "Particle size control of a monodisperse spherical Y_2O_3: Eu^{3+} phosphor and its photoluminescence properties," *Journal of Materials Research*, vol. 22, no. 7, pp. 2017–2024, 2007.

[16] M. C. Mascolo, Y. Pei, and T. A. Ring, "Room temperature co-precipitation synthesis of magnetite nanoparticles in a large pH window with different bases," *Materials*, vol. 6, no. 12, pp. 5549–5567, 2013.

[17] T. Sato and T. Nakamura, "Studies of the crystallisation of gallium hydroxide precipitated from hydrochloric acid solutions by various alkalis," *Journal of Chemical Technology and Biotechnology*, vol. 32, no. 3, pp. 469–475, 1982.

[18] H.-S. Qian, P. Gunawan, Y.-X. Zhang, G.-F. Lin, J.-W. Zheng, and R. Xu, "Template-free synthesis of highly uniform α-GaOOH spindles and conversion to α-Ga_2O_3 and β-Ga_2O_3," *Crystal Growth & Design*, vol. 8, no. 4, pp. 1282–1287, 2008.

[19] G. Li, C. Peng, C. Li et al., "Shape-controllable synthesis and morphology-dependent luminescence properties of GaOOH:Dy^{3+} and β-Ga_2O_3:Dy^{3+}," *Inorganic Chemistry*, vol. 49, no. 4, pp. 1449–1457, 2010.

[20] G. Liu, X. Duan, H. Li, and D. Liang, "Preparation and photoluminescence properties of Eu-doped Ga_2O_3 nanorods," *Materials Chemistry and Physics*, vol. 110, no. 2-3, pp. 206–211, 2008.

[21] C. Lu, L. Qi, J. Yang, D. Zhang, N. Wu, and J. Ma, "Simple template-free solution route for the controlled synthesis of $Cu(OH)_2$ and CuO nanostructures," *Journal of Physical Chemistry B*, vol. 108, no. 46, pp. 17825–17831, 2004.

[22] G. Gnanaprakash, J. Philip, T. Jayakumar, and B. Raj, "Effect of digestion time and alkali addition rate on physical properties of magnetite nanoparticles," *Journal of Physical Chemistry B*, vol. 111, no. 28, pp. 7978–7986, 2007.

[23] J. Liu, X. Du, Y. Yang, Y. Deng, W. Hu, and C. Zhong, "A one-step, clean, capping-agent-free electrochemical approach to prepare Pt nanoparticles with preferential (100) orientation and their high electrocatalytic activities," *Electrochemistry Communications*, vol. 58, pp. 6–10, 2015.

[24] T. S. Ahmadi, Z. L. Wang, T. C. Green, A. Henglein, and M. A. El-Sayed, "Shape-controlled synthesis of colloidal platinum nanoparticles," *Science*, vol. 272, no. 5270, pp. 1924–1926, 1996.

[25] C. Henrist, J.-P. Mathieu, C. Vogels, A. Rulmont, and R. Cloots, "Morphological study of magnesium hydroxide nanoparticles precipitated in dilute aqueous solution," *Journal of Crystal Growth*, vol. 249, no. 1-2, pp. 321–330, 2003.

[26] Y. Zhao, R. L. Frost, J. Yang, and W. N. Martens, "Size and morphology control of gallium oxide hydroxide GaO(OH), nano- to micro-sized particles by soft-chemistry route without surfactant," *Journal of Physical Chemistry C*, vol. 112, no. 10, pp. 3568–3579, 2008.

[27] S. Krehula, M. Ristić, S. Kubuki, Y. Iida, M. Fabián, and S. Musić, "The formation and microstructural properties of uniform α-GaOOH particles and their calcination products," *Journal of Alloys and Compounds*, vol. 620, pp. 217–227, 2015.

[28] Y. Wang, A. Muramatsu, and T. Sugimoto, "FTIR analysis of well-defined α-Fe_2O_3 particles," *Colloids and Surfaces A: Physicochemical and Engineering Aspects*, vol. 134, no. 3, pp. 281–297, 1998.

[29] Y. Quan, D. Fang, X. Zhang, S. Liu, and K. Huang, "Synthesis and characterization of gallium oxide nanowires via a hydrothermal method," *Materials Chemistry and Physics*, vol. 121, no. 1-2, pp. 142–146, 2010.

[30] Y. Park, Y. Na, D. Pradhan, B.-K. Min, and Y. Sohn, "Adsorption and UV/Visible photocatalytic performance of BiOI for methyl orange, Rhodamine B and methylene blue: Ag and Ti-loading effects," *CrystEngComm*, vol. 16, no. 15, pp. 3155–3167, 2014.

[31] Y. Hou, J. Zhang, Z. Ding, and L. Wu, "Synthesis, characterization and photocatalytic activity of β-Ga_2O_3 nanostructures," *Powder Technology*, vol. 203, no. 3, pp. 440–446, 2010.

[32] M. Muruganandham, R. Amutha, M. S. M. A. Wahed et al., "Controlled fabrication of α-GaOOH and α-Ga_2O_3 self assembly and its superior photocatalytic activity," *The Journal of Physical Chemistry C*, vol. 116, no. 1, pp. 44–53, 2012.

[33] C.-C. Huang and C.-S. Yeh, "GaOOH, and β- and γ-Ga_2O_3 nanowires: preparation and photoluminescence," *New Journal of Chemistry*, vol. 34, no. 1, pp. 103–107, 2010.